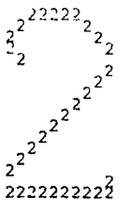

EXPERIMENTAL DETAILS AND RESULTS

The experiment on the measurement of (p,n) reaction excitation function was performed with the Van de Graaff accelerator at Trombay. The experimental arrangement, consisting of the accelerator delivering proton beams with an energy definition of $\pm$ 1 keV and a beam transport system focussing the beam onto a target (of thickness about a few micrograms/cm^2) surrounded by a number of neutron proportional counters giving effectively a 4π solid angle of detection, is described in detail in the first three sections of the present chapter. The following two sections are devoted to a description of the method used to calibrate the accelerator for determining the beam energy and the procedure adopted to measure the absolute (p,n) cross sections along with error estimates. The results obtained for both the fine structure and smooth excitation functions are described in the last section for the two nuclei (^{55}Mn and ^{80}Se) studied.

2.1 ACCELERATOR AND BEAM TRANSPORT SYSTEM

The 5.5 MeV Van de Graaff generator at Trombay[23] is a single stage vertical type positive ion accelerator supplied by the High Voltage Engineering Corporation, USA. The machine is capable of delivering beams of protons, deuterons, ^3He and α-particles. The high voltage terminal is a well polished stainless steel dome. The voltage is generated by a continuous transfer of positive charge by means of a motor driven conveyer belt. To provide insulation, the whole assembly is housed in a larger pressure tank containing a mixture of CO_2 and N_2 gas (in the ratio 1:4) at 220 psi pressure. Positive ions are produced by means of a RF ion source. These ions enter the accelerator tube and are accelerated by the terminal voltage. A uniform voltage gradient is maintained over this path by means of a set of equi-potential rings. The beam tube is made of glass and a vacuum of the order of 10^{-6} torr is maintained in it.

The accelerated beam travelling vertically downwards is deflected through 90° and brought in the horizontal plane by an analysing magnet, which has a field stability of 0.005%. A fraction of the accelerated beam coming out of the analysing magnet assembly is intercepted by each of the two edges of a 20 mil wide control slit connected to earth via variable input resistors of a feedback amplifier. This slit serves the dual purpose of defining the energy spread and stabilising the energy of the beam. When the analysing magnet is set at a specific field for a given energy of the beam and the dome voltage is held at the appropriate value, the beam going down is intercepted equally by the edges of the slit so that the differential voltage between them is zero. Any change in the dome voltage causes the

beam spot to move across the slit, producing voltage signals at the input of the differential amplifier. The output of this differential amplifier is used as a negative feedback to vary suitably the bias on a corona load which brings the dome voltage back to the desired value. This arrangement has resulted in stabilising the energy of the beam to better than 0.1%.

The magnetic field of the analysing magnet is monitored by a proton NMR gaussmeter. The NMR probe uses the proton resonance technique to determine the deflecting field which is proportional to the resonance frequency. The particle energy E (in MeV) is related to the measured frequency f (in MHz) by the relation

$$E \left(1 + \frac{E}{E_0} \right) = K f^2 Z^2/M \qquad \ldots \qquad (2.1)$$

where Z, M and E_0 are the charge, mass (in amu) and the rest mass (in MeV) respectively of the accelerated particle and K is the calibration constant. The resonance frequency is measured with a high precision frequency counter (Hewlett Packard model 5245L frequency meter). The determination of the calibration constant by measuring known (p,n) thresholds[24] is described in section 2.4.

The accelerated and focussed beam passes through the analysing magnet and a five port switching magnet assembly and enters the experimental beam port placed at 45° from the central direction. The port is aligned with respect to the beam direction so that the beam travels along the axis of the long tube assembly. This alignment is checked by mounting a quartz plate at several intersections of the port and observing the flourecent spot of the beam. Further downstream, the beam is focussed by a pair of magnetic quadrupole lenses and collimated by a pair of 2 mm dia circular tantalum

apertures. Finally this well collimated and focussed beam falls on the target kept at the end of the beam port.

2.2 TARGETS

Targets in the thickness range of a few micrograms/cm^2 were prepared by vacuum deposition of thin films of manganese and selenium metals onto thick tantalum backings. Tantalum backings were used in all the cases to reduce neutron background. The backing was kept thick enough to stop the beam and thus also acted as the Faraday cup. Spectroscopic pure natural manganese (100% ^{55}Mn, other metallic impurities being less than 20 ppm) and 93% enriched ^{80}Se (obtained from ORNL) were used for preparing targets. The thickness of the tantalum backing was 0.15 mm. The backings were properly cleaned and mounted in a vacuum evaporation chamber directly above the material at a height of about 25 cm. The material was kept in a tantalum boat which was electrically heated. A vacuum of the order of 10^{-5} torr was maintained during evaporation. The heating current was gradually increased using a variac, the rate of increase being kept very slow near the melting point of the metal to ensure uniform deposit.

The target thickness in terms of energy loss was determined[25] in all the cases from the shift in the edge of the spectra due to the back-scattered low energy (about 2 MeV) α- particles from blank tantalum and from tantalum covered with the thin substrate of the target metal. The targets were mounted in a scattering chamber for this purpose and a silicon surface barrier detector mounted at a sufficiently large backward angle ($\sim 160^{\circ}$) with respect to the incident beam was used to detect the scattered α- particles. Referring to the schematic representation in fig. (2.1a),

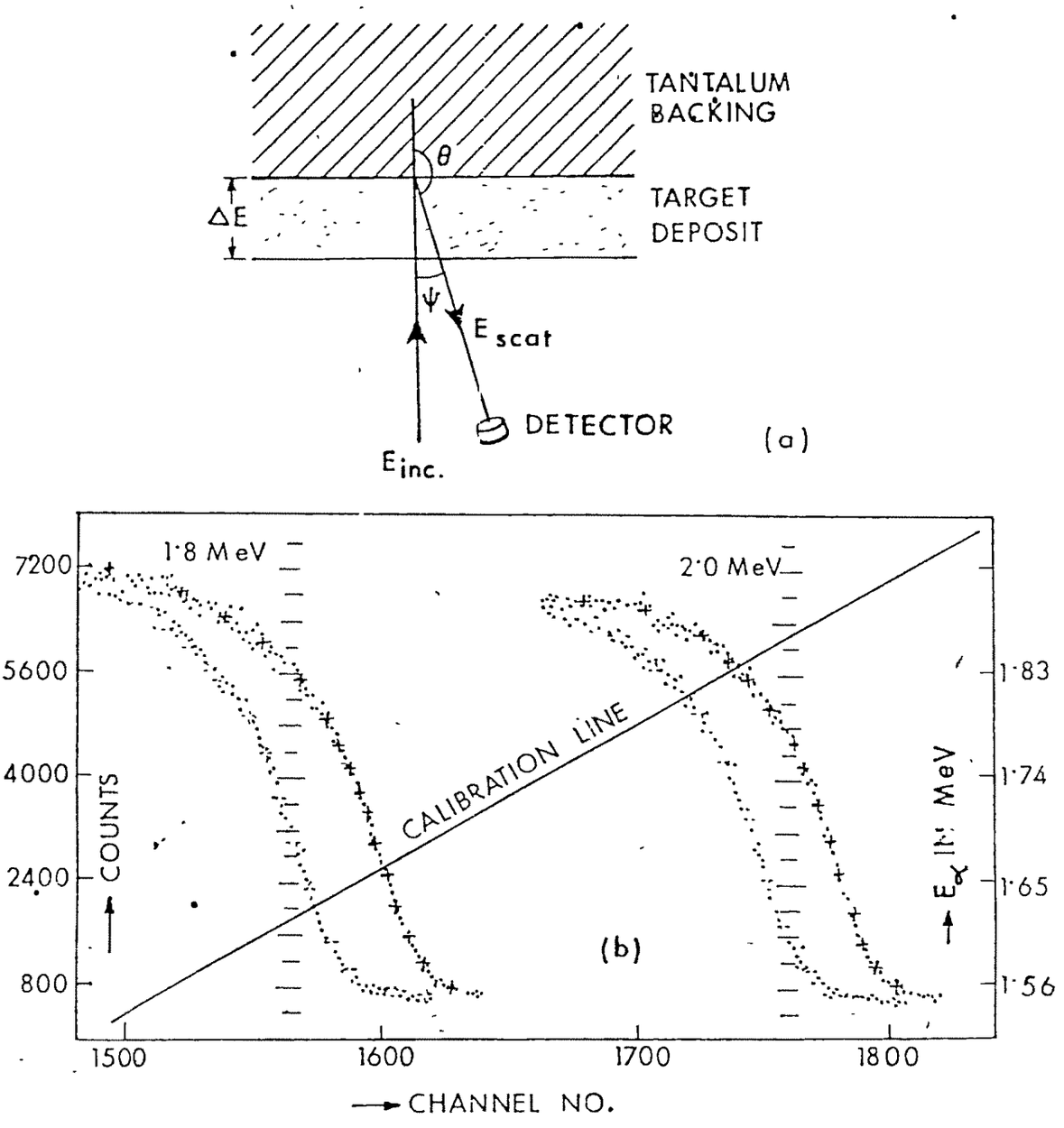

Fig. (2.1) : (a) A schematic sketch of the scattering of α-particles for target thickness measurement, (b) detector spectrum for blank Ta (dots with crosses) and Ta covered with target film (dots alone). The scale on the right side is for detector calibration.

6251

the total shift in energy would be equal to $\Delta E\ (1 + \sec \psi)$, where $\psi = 180^{\circ} - \theta$ and ΔE is the energy loss in the target substrate for an energy E of the projectile taken to be the mean of the incident and scattered energies. The back scattered spectrum from blank tantalum and from tantalum having the target film on it are shown in fig. (2.1b) for two different energies of α- particles in one of the measurements. By this method, target thicknesses were measured with an accuracy of better than 15%.

2.3 DETECTOR AND ELECTRONICS

The detector assembly for neutrons consists of a cube of paraffin in which twelve $^{10}BF_3$ - filled proportional counters are embedded.[26] The counters are arranged in two coaxial cylindrical layers around the target with the beam direction as the common axis so that they subtend nearly 4π solid angle for neutrons emitted from the target kept at the centre of the paraffin block. The paraffin serves to moderate the neutrons so that they may be effectively detected by the BF_3 counters. The efficiency of this detector assembly has been measured earlier[27] as a function of energy with an accuracy of better than 7%. The counter has a flat response for neutrons upto 1 MeV energy, the efficiency being about 10%. At higher neutron energies, the efficiency falls down almost linearly.

A schematic arrangement of the 4π neutron counter along with the necessary electronics support is shown in fig. (2.2). The signals from the inner and outer sets of counters were separately processed by a combination of a preamplifier and a linear non-overload amplifier. The signals were finally counted by decade scalers having a range of ten decades. The target assembly placed at the centre of the paraffin block was kept insulated from the beam port and acted as the Faraday cup.

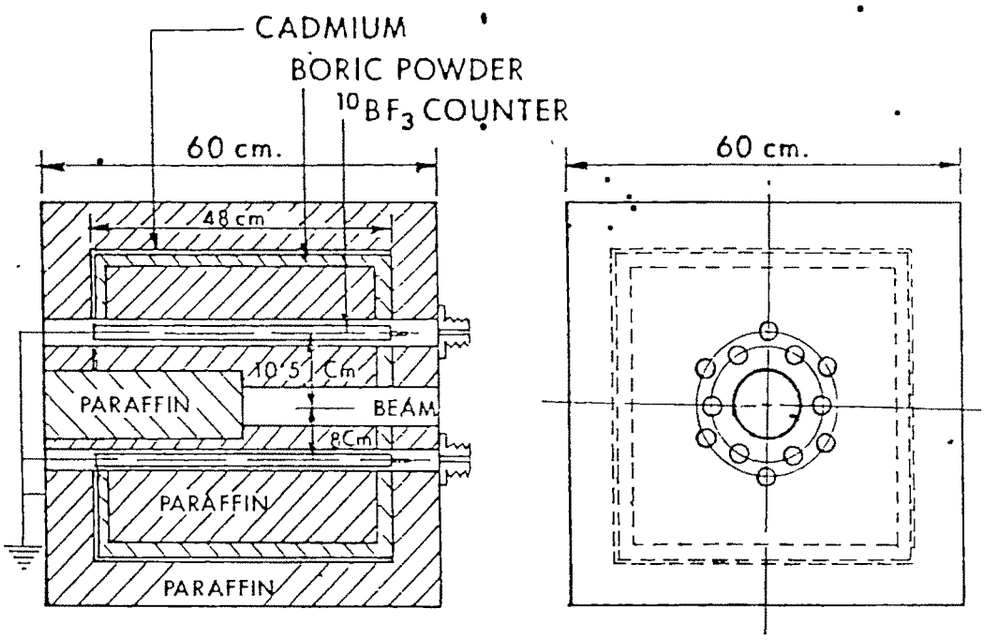

(a) 4π NEUTRON COUNTER

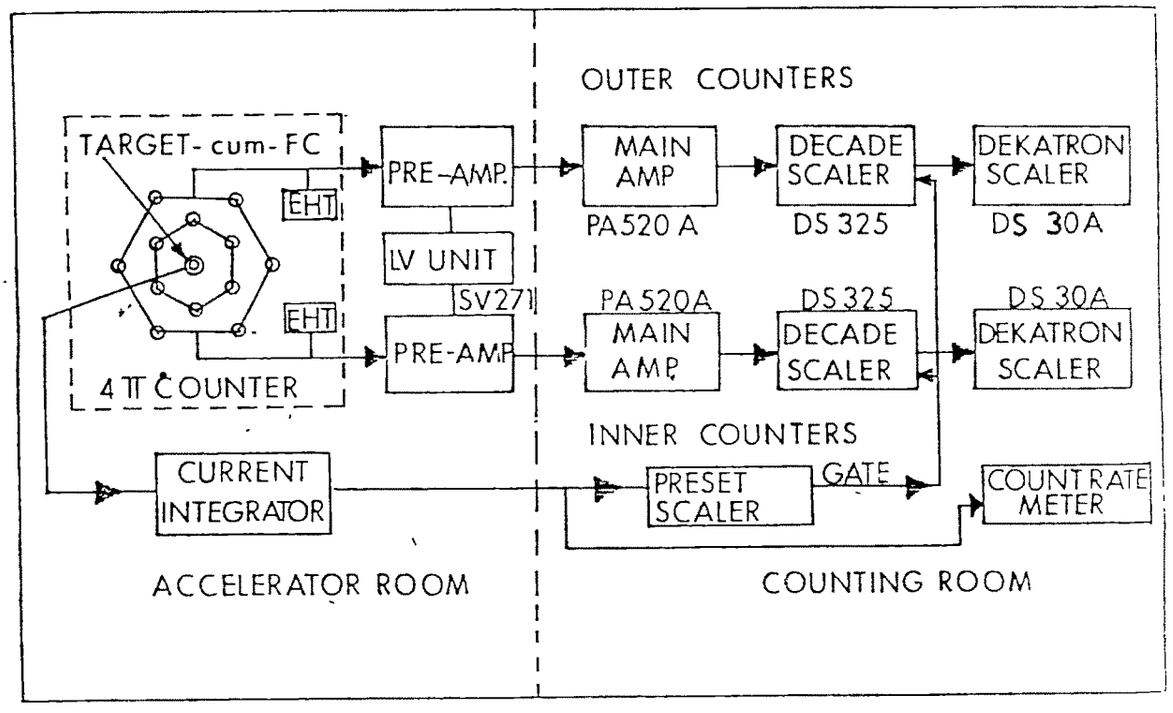

(b) BLOCK DIAGRAM OF ELECTRONICS

Fig. (2.2) : Schematic arrangement of the neutron detector and associated electronics support for measuring the relative neutron yield.

The proton beam current was measured by a current integrator[28]. The current integrator signals were counted by a scaler which could be controlled for a preset number of counts corresponding to a given accumulated charge. The preset scaler generated a gate signal which actuated the decade scalers counting the inner and outer counters. The current integrator was also connected to a count rate meter, in parallel with the preset scaler, to give an approximate idea of the magnitude of the current. This was necessary for monitoring the beam, in particular to keep the current low enough so that the target substrate did not deteriorate due to overheating caused by an unnecessarily large current. The current integrator was calibrated using a standard current source.

The neutron yield measured utilising the 4π geometry counter is summed over all neutron groups produced in the reaction. It must be pointed out that if the neutrons produced in the reaction were strongly anisotropic, the counting rate would depend on the angular distribution, even though the paraffin moderator of the neutron detector tends to average over angles. In the present experiments, however, it is assumed that the (p,n) reactions have almost isotropic yields to make the counting rate a direct measure of the total yield. This should be a good assumption since protons of energy less than 5.5 MeV bombarding medium weight nuclei produce small recoil velocity and the (p,n) reaction proceeds primarily by compound nucleus formation.[2]

Further, the energy of the ground state neutron group is usually taken as the effective energy of the neutrons produced for efficiency calculations. This will be a good approximation as long as the energies of the various neutron groups populated are less than or of the order of 1 MeV. This is due to the fact that the detection efficiency is fairly constant

with neutron energy upto 1 MeV. As one goes to higher energies the detector efficiency starts decreasing slowly. Then the above mentioned assumption of using the ground state neutron energy as the effective energy for efficiency calculation may not be very reliable, resulting in an overestimate of the cross section. However, it is difficult to estimate the error involved in this procedure as it requires not only the energies of various neutron groups but also their relative intensities which are usually unknown. For the present experiment, the energies of the outgoing neutrons are still small enough that even one or two collisions in the paraffin moderator is sufficient to reduce the energies of neutrons to less than 1 MeV to be detected with adequate efficiency. This problem is, therefore, not expected to seriously affect the results of the present experiment.

2.4 ACCELERATOR CALIBRATION

To determine the energy (in MeV) of the accelerated protons from the measured frequency of the NMR gaussmeter, the calibration constant K in eqn. (2.1) must be determined. The constant K is related to the magnetic moment of the proton and the radius of curvature of the beam path in the analysing magnet. The calibration of the accelerator for the present experiment was done by measuring the threshold energy of the ^{7}Li (p,n) ^{7}Be reaction and comparing it with the known value of 1.8806 MeV.[24]

An HH^{+} beam from the Van de Graaff machine was allowed to fall on a natural LiF target. Neutrons were detected using the 4π counter. The beam was monitored with a current integrator using the target holder as the Faraday cup. The neutron yield for a preset value of the current integrator count was measured as a function of the NMR frequency. After approximately locating the threshold for neutron emission, the NMR frequency was varied

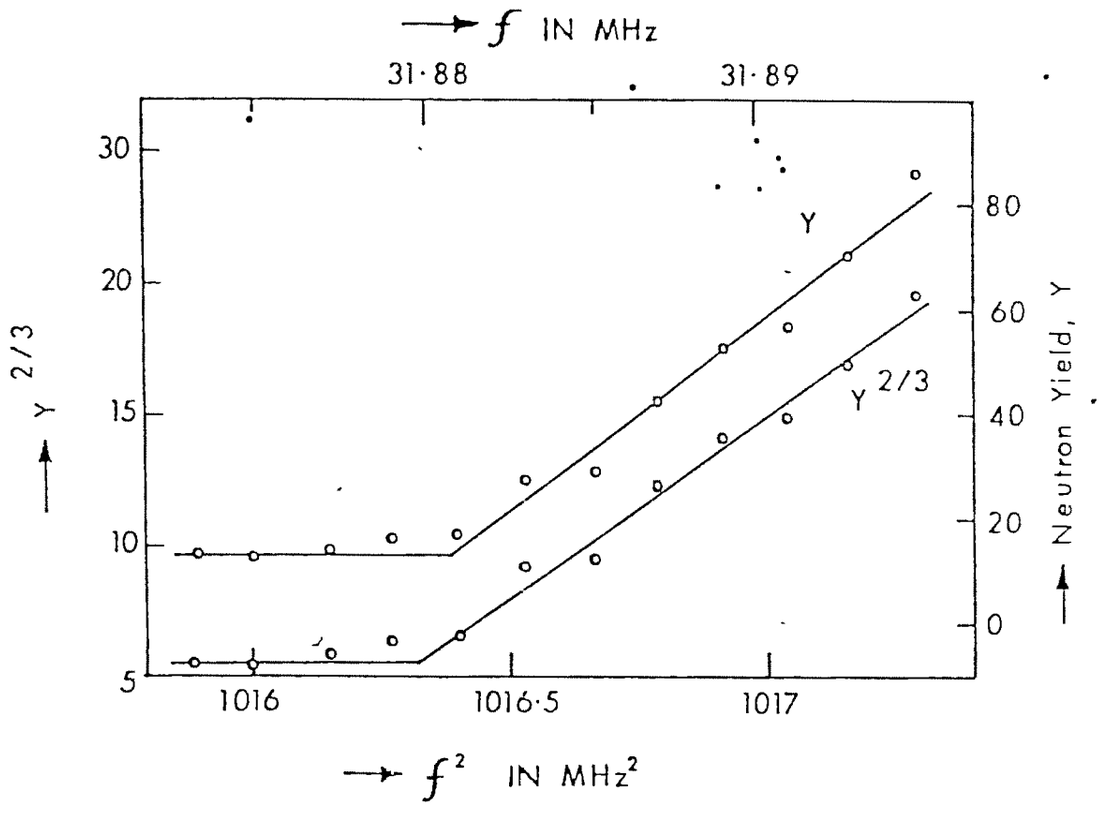

Fig. (2.3) Yield curve for the reaction ^{7}Li (p,n)^{7}Be as a function of NMR frequency to determine the accelerator calibration constant.

in steps of 2 KHz. In this way, the yield curve shown in fig. (2.3) was obtained. The threshold is best located by plotting $Y^{2/3}$ against f^2, where Y is the yield corresponding to the NMR frequency f. This is because thick target measurement of the total reaction cross section should produce an yield curve that varies as $(E - E_{th})^{3/2}$, where E_{th} is the threshold energy.

From the $Y^{2/3}$ vs. f^2 curve, the NMR frequency corresponding to the (p,n) threshold is found to be 31800 KHz. Using the value of E_{th} = 1.8806 MeV in eqn. (2.1) for the threshold of the ^{7}Li (p,n)^{7}Be reaction, the value of the calibration constant was obtained as K = 0.0074 MeV per MHz^2. If the same procedure were used for the simple yield curve (Y vs. f^2), a slightly higher value of K would be obtained.

2.5 MEASUREMENT OF ABSOLUTE (p,n) CROSS SECTION

2.5.1 Measurement of Relative Neutron Yield

After the proton beam was properly aligned upto the collimator slits and the calibration constant determined, the target of interest was mounted in the target holder kept at the end of the beam port. The beam port was kept under vacuum of the order of 10^{-5} torr using several oil diffusion pumps. Beam energy was varied first in steps of 5 keV. After each change in energy, the analysing magnet was allowed to stabilise before the counting of neutrons was started. For energies less than 1.5 MeV, a beam of HH^+ ion was used at double the required energy of protons (the HH^+ ion breaks into two protons of equal energy in the field of target atoms). At the higher dome voltages around 5 MeV, the machine became very unstable and required a longer time of stabilization before counting could be done.

Relative neutron yield was first measured at a given energy by counting the neutron pulses from the 4π counter using decade scalers. In the first scan over the entire range of energy, targets of thicknesses of the order of 5 keV for 4 MeV protons were used. The count rate meter gave a rough analog indication of the beam current which was kept around 50 - 100 nA for a reasonable count rate. The decade scalers counting the neutron pulses from the 4π counter were gated by the preset scaler counting a fixed number of integrated charge. Beam current was reduced near resonances to avoid very high counting rates and the resulting dead time corrections.

Background neutron yield was recorded at regular intervals of about 100 keV change in energy by turning the target by 180° so that the tantalum backing faced the beam. Reproducibility of data was checked by repeating the measurements at frequent intervals by going down in energy and scanning

the relative yield over about 100 keV range, particularly in the flat regions of the excitation function. This also provided a check against the possible deterioration of the target. The ratio of the yields in the inner and outer sets of counters was monitored throughout as a check against possible malfunctioning of the electronics system.

For the measurement of neutron yield near prominent resonances, thinner targets of the order of 1 keV for 2 MeV protons were used in both the manganese and selenium cases. The beam energy was varied in smaller steps (1 keV for ^{55}Mn and 2.5 keV for ^{80}Se). After each change in energy, the analysing magnet current was allowed to stabilise properly. Measurements were made by making several passes up and down the resonance to average out the effects of target non-uniformities and beam energy fluctuations. An example of good reproducibility in scanning the resonance is shown in fig. (3.3) for the case of ^{55}Mn (p,n)^{55}Fe reaction.

2.5.2 Estimation of Absolute Cross Section

The relative neutron yield thus obtained was converted to the absolute yield Y by correcting for the dead time losses and then subtracting the background contribution. For this purpose, the background yields measured at several energies were fitted with a smooth polynomial and this polynomial was used to predict the background yield at other energies on a point-to-point basis. The current integrator was calibrated using a standard current source. Knowing the target thickness in terms of the number of atoms per cm^2, the absolute cross section σ was calculated using the standard relation[24]

$$Y = N_t N_p \sigma \varepsilon \qquad \ldots \qquad (2.2)$$

where N_t is the number of target atoms per cm^2, N_p is the number of protons incident on the target and ε is the efficiency of the neutron counter at the appropriate energy. As explained in sec. (2.3), the efficiency ε was

estimated as a function of neutron energy corresponding to the ground state neutron group.

The absolute maximum error in the total (p,n) cross section was esimated to be 20%, comprising of errors in :

(a) target thickness measurement, 15%

(b) target non-uniformity, 5%

(c) efficiency of the neutron counter, 7%

(d) beam current integration, 1% and

(e) counting statistics, 2% .

The relative point-to-point error was 5% mainly due to target non-uniformities.

2.6 EXPERIMENTAL RESULTS

2.6.1 Resonances in ^{55}Mn (p,n) ^{55}Fe Reaction

The fine structure excitation function for the reaction ^{55}Mn (p,n) ^{55}Fe measured from E_p = 1.35 MeV to 5.42 MeV[29] is shown in fig. (2.4). It exhibits strong resonances as well as weaker fine structure having widths of the order of 5 - 10 keV. The prominent resonances seen in the present experiment, which are expected to be the analogs of the levels in the parent nucleus ^{56}Mn, are listed in the first part of Table 2.1 along with the corresponding excited states of ^{56}Mn and the ℓ- value of the neutron obtained from the ^{55}Mn (d,p) ^{56}Mn reaction studies. The arrows in fig. (2.4) indicate other expected isobaric analog resonances (IARs) assuming the Coulomb displacement energy ΔE_c (^{56}Fe - ^{56}Mn) to be 8.590 MeV.[30] The IARs observed in the lower energy region by previous workers[12,13] are also seen in the present work, except for the analog of the ground state of ^{56}Mn which is expected around 1.34 MeV as this energy region has not been covered in

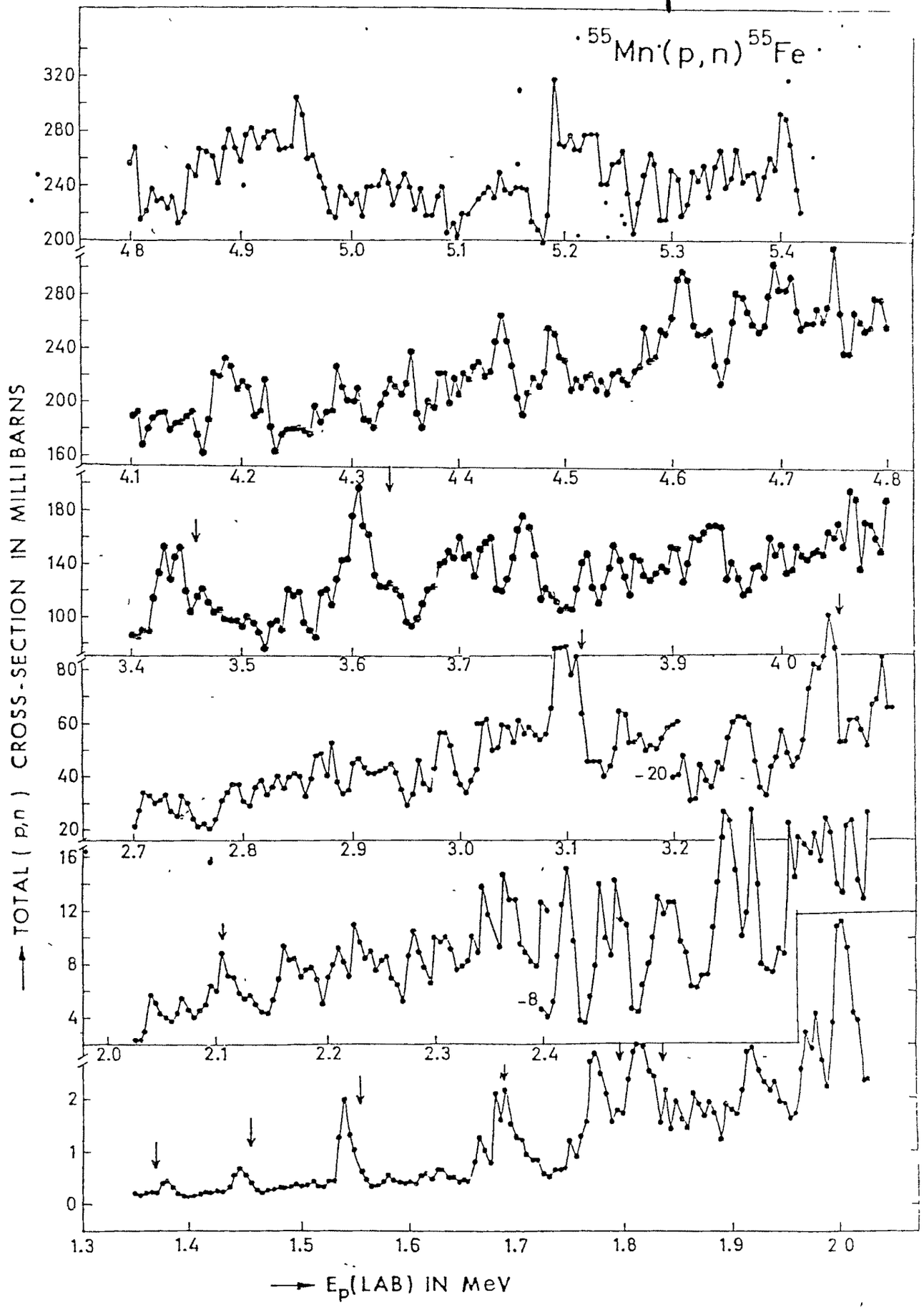

Fig. (2 4) Fine structure excitation function for the reaction ^{55}Mn (p n)^{55}Fe measured in 5 keV steps from E_p = 1.35 to 5.42 MeV. The arrows indicate the expected positions of IARs based on the Coulomb energy shift = 8.590 MeV. Note the change in cross section scale at 2.4 and 3.2 MeV.

TABLE 2.1

Prominent IARs observed in the present experiment

E_p(lab) in MeV	Excitation energy of the parent nucleus in MeV	J^π	ℓ_n
	Reaction ^{55}Mn (p,n) ^{55}Fe		
1.390	0.026	2^+	1
1.456	0.110	1^+	1
1.543	0.214	$(2^+,4^+)$	1 (3)
3.610	2.254	-	1
	Reaction ^{80}Se (p,n) ^{80}Br		
3.832	0. (g.s.)	$\frac{1}{2}^-$	1
4.311	0.469	$\frac{3}{2}^-$	1
4.874	1.053	$\frac{5}{2}^+$	2
5.016	1.234	$\frac{1}{2}^+$	0
5.098	1.304	$\frac{5}{2}^+$	2
5.245	1.407	$\frac{3}{2}^-$	1

the present work. A discussion of the prominent resonances is given below.

1.54 MeV Resonance :- The strong resonance measured at 1.54 MeV incident proton energy and shown in fig. (2.4) can be identified with the IAR formed by an ℓ=1 proton leading to a 2^+ level in the compound nucleus ^{56}Fe which is the analog of the 0.213 MeV level in the parent nucleus ^{56}Mn, studied through the ^{55}Mn (d,p) ^{56}Mn reaction.[31] However, subsequent (n,γ) measurement[32] on ^{55}Mn has revealed that the parent state in question is a doublet with energies 0.212 and 0.215 MeV and with spins 4^+ and 1^+ or 2^+ respectively. Similarly the study[13] of the reaction ^{55}Mn (p,γ) ^{56}Fe has

shown that there are two levels in ^{56}Fe at excitation energies E_x = 11.699 and 11.705 MeV with spins 4^+ and 2^+ respectively, which could be the isobaric analogs of the 0.212 and 0.215 MeV levels in ^{56}Mn.

In the present (p,n) experiment, as the energy resolution is better than 2 keV, the two levels separated by 6 keV as measured in (p,γ) work should have been seen distinctly. However, there is no evidence of a second resonance in the neighbourhood of the peak at 1.543 MeV as seen in fig. (2.4) where the width of the resonance is only about 3 keV. Considering the spins of the levels concerned, it can be seen that the 4^+ level (the lower of the doublet) would be only weakly excited as a resonance in the (p,n) excitation function because of the highly reduced penetrability of the corresponding ℓ=3 partial wave for the outgoing neutron channel.

Assuming that only the ground state of the residual nucleus ^{55}Fe (with $J^\pi = \frac{3}{2}^-$) would be energetically open for 1.54 MeV protons, the outgoing neutron from the 4^+ IAR would have an energy of only 400 keV and would have to carry an angular momentum of three units. The penetrability for this partial wave would be almost negligible compared to that for the neutron coming out due to the decay of the 2^+ IAR which would have similar energy but would have to carry away an angular momentum of only one unit. Thus the observed single strong resonance could be interpreted as the analog of the 0.215 MeV 2^+ state of the parent nucleus ^{56}Mn. This is in fact supported by the (p,n) and (p,γ) measurements of Otto et al[12] where one finds only one structure at this proton energy in the (p,n) excitation function but more than one structure in the case of (p,γ) reaction.

3.6 MeV Resonance :- The resonance appearing around E_p = 3.61 MeV is also strong and can be attributed to the 2.254 MeV level of ^{56}Mn. This state is populated by an ℓ=1 neutron in the ^{55}Mn (d,p)^{56}Mn reaction with sufficient strength.[31] However, in the present experiment, the structure

seen around the 3.6 MeV peak is not very clean and this makes the strength of the resonance relatively weak. This also indicates that the special significance of the IAR is lost as the excitation energy increases. This resonance has, therefore, not been included in subsequent spectroscopic analysis.

2.6.2 Resonances in ^{80}Se (p,n) ^{80}Br Reaction

The fine structure excitation function for the reaction ^{80}Se (p,n) ^{80}Br measured from E_p = 2.6 MeV to 5.4 MeV[33] is shown in fig. (2.5). The lower energy region does not contain any resonances and is shown separately. Beyond 3.7 MeV incident energy, the excitation function shows several prominent resonances, most of which have been reported earlier.[16] The IARs observed in the present experiment are listed in the second part of Table 2.1 along with the corresponding excited states of the parent nucleus ^{81}Se and the neutron ℓ- values obtained from the (d,p) reaction studies.[17] All these IARs have been studied in detail using thinner targets and in finer steps of beam energy of about 2.5 keV.

The IAR at E_p = 5.245 MeV has been observed for the first time in the present experiment. The weaker IAR around 4.2 MeV could not be seen in elastic scattering experiment.[16] This fact provides a good justification of studying IARs through (p,n) reactions. As discussed in sec. 1.5, (p,n) reactions are specially suited for such studies particularly at sub-Coulomb energies where the proton partial width in the exit channel is very small.

2.6.3 Smooth Excitation Functions

The fine structure excitation functions for both the nuclei were averaged over 100 keV energy interval to smoothen out the compound nuclear fluctuations and obtain the excitation function corresponding to the "thick

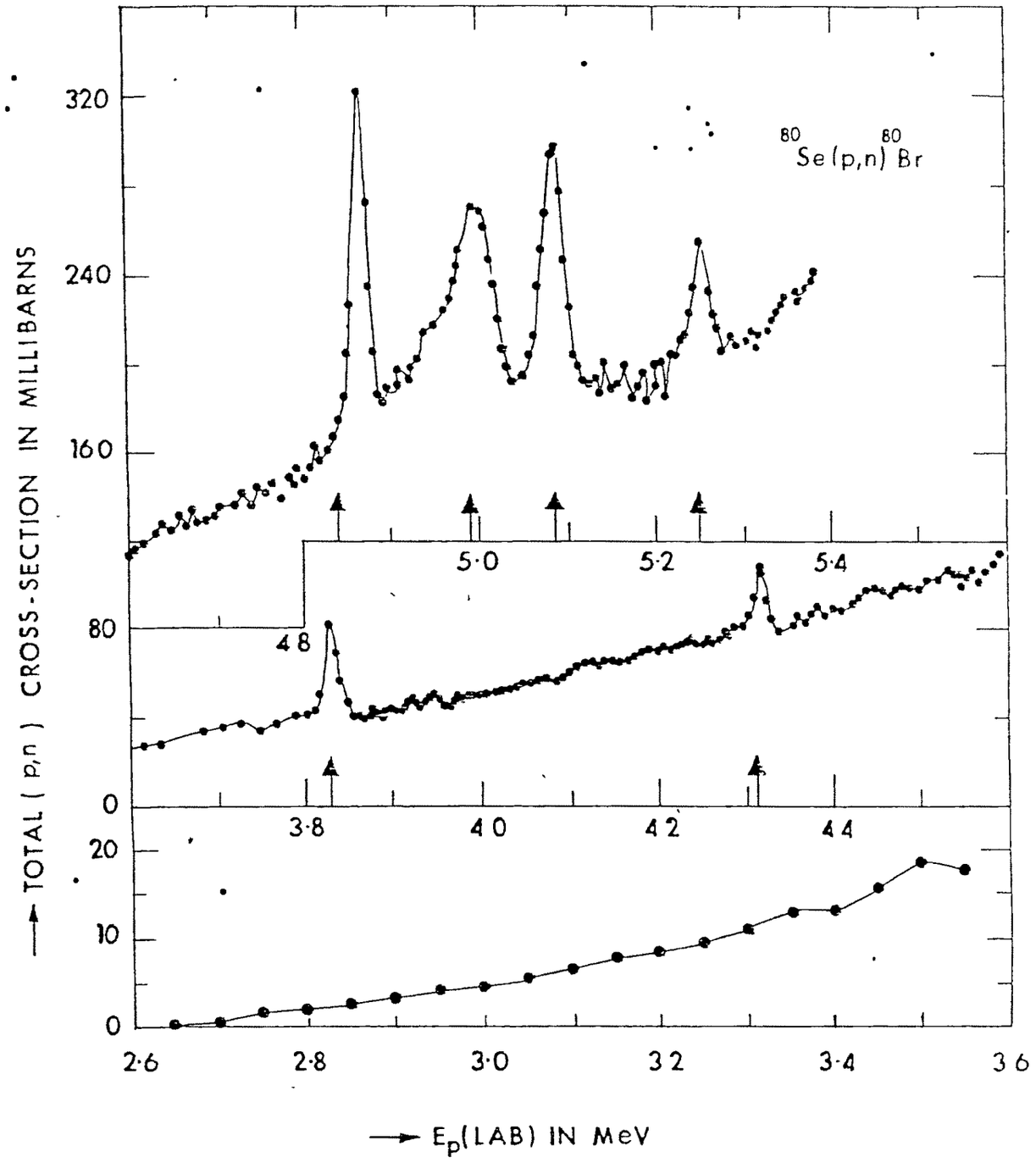

Fig. (2.5) Fine structure excitation function for the reaction $^{80}Se\ (p,n)^{80}Br$ measured in 5 keV steps from E_p = 2.6 to 5.4 MeV. The arrows indicate the expected positions of IARs based on the Coulomb energy shift = 10.45 MeV.

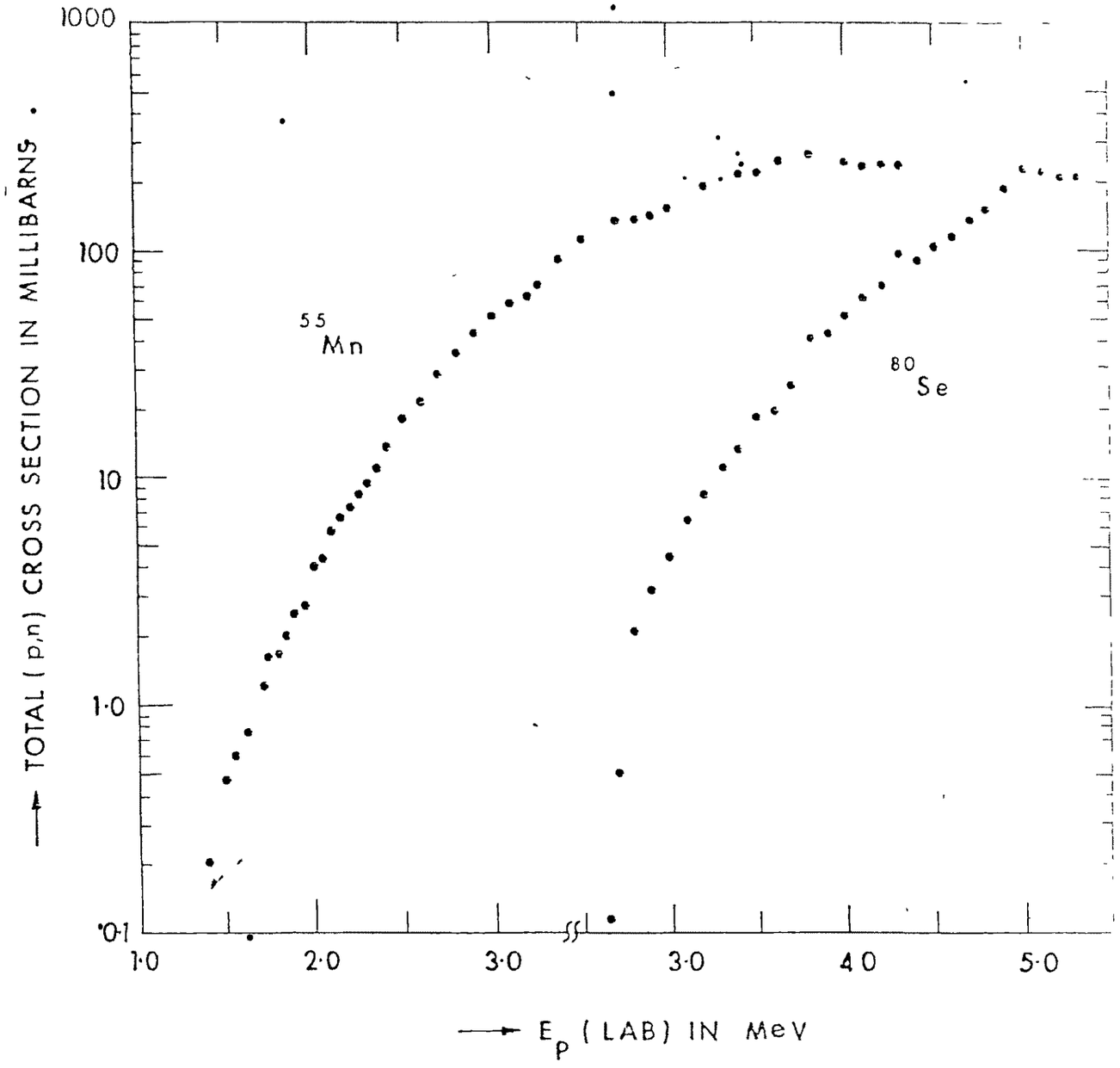

Fig. (2.6) : Smooth (p,n) excitation functions for ^{55}Mn and ^{80}Se.

target" case suitable for optical model analysis. The averaged excitation functions are shown in fig. (2.6) on a semi-log scale to show the exponential rise of the (p,n) cross section as a function of energy. The average cross section values agree well with the thick target measurements of Johnson et al.[14] The excitation functions are almost structureless and donot show the presence of any intermediate width states.[34]